Biosensors and Bioelectronics 189 (2021) 113356

Contents lists available at ScienceDirect

Biosensors and Bioelectronics

journal homepage: www.elsevier.com/locate/bios

Label-free E-DNA biosensor based on PANi-RGO-G*NPs for detection of cell-free fetal DNA in maternal blood and fetal gender determination in early pregnancy

Mahdi Malmir [a], Jalal Arjomandi [a,b,*], Abolfazl Ghafouri Khosroshahi [c], Mohammadreza Moradi [d], Hu Shi [b]

[a] Department of Physical Chemistry, Faculty of Chemistry, Bu-Ali Sina University, 65178, Hamedan, Iran
[b] School of Chemistry and Chemical Engineering, Shanxi University, Taiyuan, China
[c] Department of Medicinal Chemistry and Nuclear Medicine, School of Pharmacy, University of Sciences, Hamedan, Iran
[d] Research Center for Molecular Medicine, Hamadan University of Medical Sciences, Hamadan, Iran

ARTICLE INFO

Keywords:
Cell-free fetal DNA
Gold nanoparticles
Maternal blood
Pregnancy
E-DNA biosensor

ABSTRACT

In this study, a DYS14 aptamer/polyaniline–reduced graphene oxide–gold nanoparticles/gold (Apt/PANi–RGO–G*NPs/Au) electrode was fabricated to detect the Y-chromosome DYS14 DNA sequence in cffDNA in the blood plasma of pregnant women and used on real and laboratory samples with high success rate. The electrochemical properties of the prepared E-DNA biosensor were characterized by CV, SWV, XRD, and EIS. The E-DNA biosensor morphological characteristics were investigated by TEM, SEM, and EDX. Phosphorothioate was used to link the aptamer to PANi–RGO–G*NPs modified gold electrode. This is due to control of the adsorption polarity and increase adsorption stability. Under optimized conditions, the linear range of the analytical technique with respect to the logarithm of the target sequence concentration was 1.0×10^{-16}–1.0×10^{-8} M, the detection limit was 4.26×10^{-17} M, and the limit of quantitation was 1.422×10^{-16} M. The E-DNA biosensor displayed high selectivity and sensitivity, high efficiency, and acceptable repeatability. For fetal sex detection, 12 pregnant women from the 5th to the 15th week of gestation participated in the study. Results indicated the fabricated Apt/PANi–RGO–G*NPs/Au E-DNA biosensor to be appropriate for fetal sex determination in pregnant women between the 7th and 9th week of gestation. Notably, this method can be used as a model for the study of pathogens like bacteria and viruses.

1. Introduction

DNA detection has a central role in several investigations that have to do with human health. Over the past two decades, non-invasive prenatal testing has made it possible to detect cell-free fetal DNA (cffDNA) in maternal blood by molecular methods, a highly desirable goal in human genetics. Currently, cffDNA fragments are detectable in the mother's blood plasma starting from the fifth week of pregnancy and until birth. Determination of the gender of the fetus early during gestation is an important therapeutic goal, especially in the case of pregnant women for whom the fetus is at increased risk of an X-chromosome-linked illness, due to genetic predisposition. In fact, pretreatment methods can, to some extent, prevent the birth of a sick baby. More than some other techniques, analysis of the cffDNA present in maternal plasma has been regarded as a non-invasive procedure for clinical applications. Indeed, implementation of more invasive methods like amniocentesis and chorionic villus sampling is associated with a 1–2% risk of miscarriage. Therefore, the opportunity for reliable genetic testing based on maternal plasma-extracted cffDNA in the early stages of pregnancy is attractive from a medical standpoint. DNA sequences SRY, DYS14, and DAZ located on the Y-chromosome are used for fetal sex determination (Zargari et al., 2011). Today, many methods have been utilized for DNA analysis, such as real-time quantitative polymerase chain reaction (qPCR) (Lun et al., 2008), quartz crystal microbalance, electrochemiluminescence, fluorescence, surface plasmon resonance spectroscopy, and electrochemistry (Huang et al., 2017). However, these methods have some limitations: they are time-consuming and high-cost, they involve complex sample treatment procedures, and require

* Corresponding author. Department of Physical Chemistry, Faculty of Chemistry, Bu-Ali Sina University, 65178, Hamedan, Iran.
E-mail addresses: j_arjomandi@yahoo.com (M. Malmir), j_arjomandi@basu.ac.ir (J. Arjomandi).

https://doi.org/10.1016/j.bios.2021.113356
Received 9 April 2021; Received in revised form 6 May 2021; Accepted 16 May 2021
Available online 26 May 2021

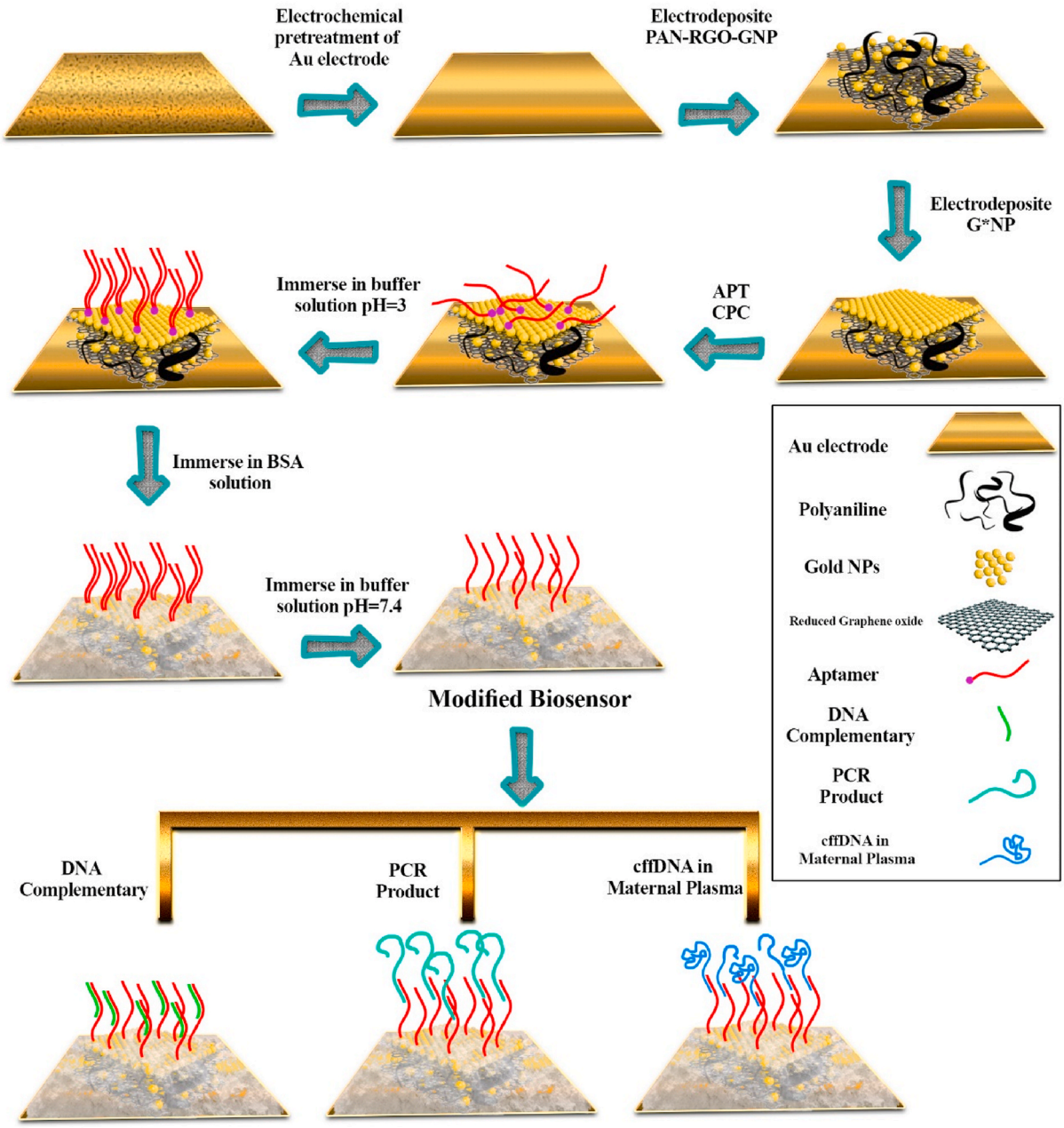

Scheme 1. Preparation of the PANi–RGO–G*NPs/Au Electrode and Fabrication of the Apt/PANi–RGO–G*NPs/Au Aptasensor.

sophisticated instrumentation and expert operators (Su et al., 2005) (Sun et al., 2017). In analytical chemistry, sensors of a range of types have attracted much attention, due to the accuracy and sensitivity that they afford, as well as their low response time, reusability, and portability. Electrochemical biosensors can be applied to detect particular biological molecules in diseases. Over the past two decades, aptamer-based biosensors (E-DNA biosensors) have been the focus of much research attention as a result of their specific properties (Xiang et al., 2020). In order to improve detection sensitivity, various immobilization techniques have been devised to probe single-strand DNA (ssDNA) sequences and to afford signal amplification; such methods include physical and electrochemical adsorption, electrochemical entrapment, and covalent immobilization (Xu et al., 2015). The steps implemented for the immobilization of the ssDNA probe at the transducer level influence various sensor parameters, such as accuracy, sensitivity, selection, and longevity. The implementation of some of these immobilization techniques is time-consuming and requires the use of electrodes modified with expensive chemicals that bind biomolecules to the modified electrode (Radhakrishnan et al., 2013). The development of nanomaterials affords additional opportunities to build E-DNA biosensors; in addition to increasing the amount of immobility, these materials speed up the transmission of electronics with excellent selection (Odeh et al., 2020). Recently, many E-DNA biosensors have been used to detect DNA hybridization, a characteristic of significant importance given its relevance to the detection of pathogens and the diagnosis of genetic diseases. In this context, E-DNA biosensors are especially interesting, due to their inherent miniaturization and low cost (Karastogianni and Girousi, 2015). E-DNA biosensors can be used to detect infectious agents early and accurately and to monitor specific sequence hybridization events directly. However, these biosensors still require sophisticated tools, pre-treatment methods, and expensive large-scale electrodes (Xu et al., 2001).

Indicator-based E-DNA biosensor typically use metals that interact with ssDNA, double-strand DNA (dsDNA), and other species, like

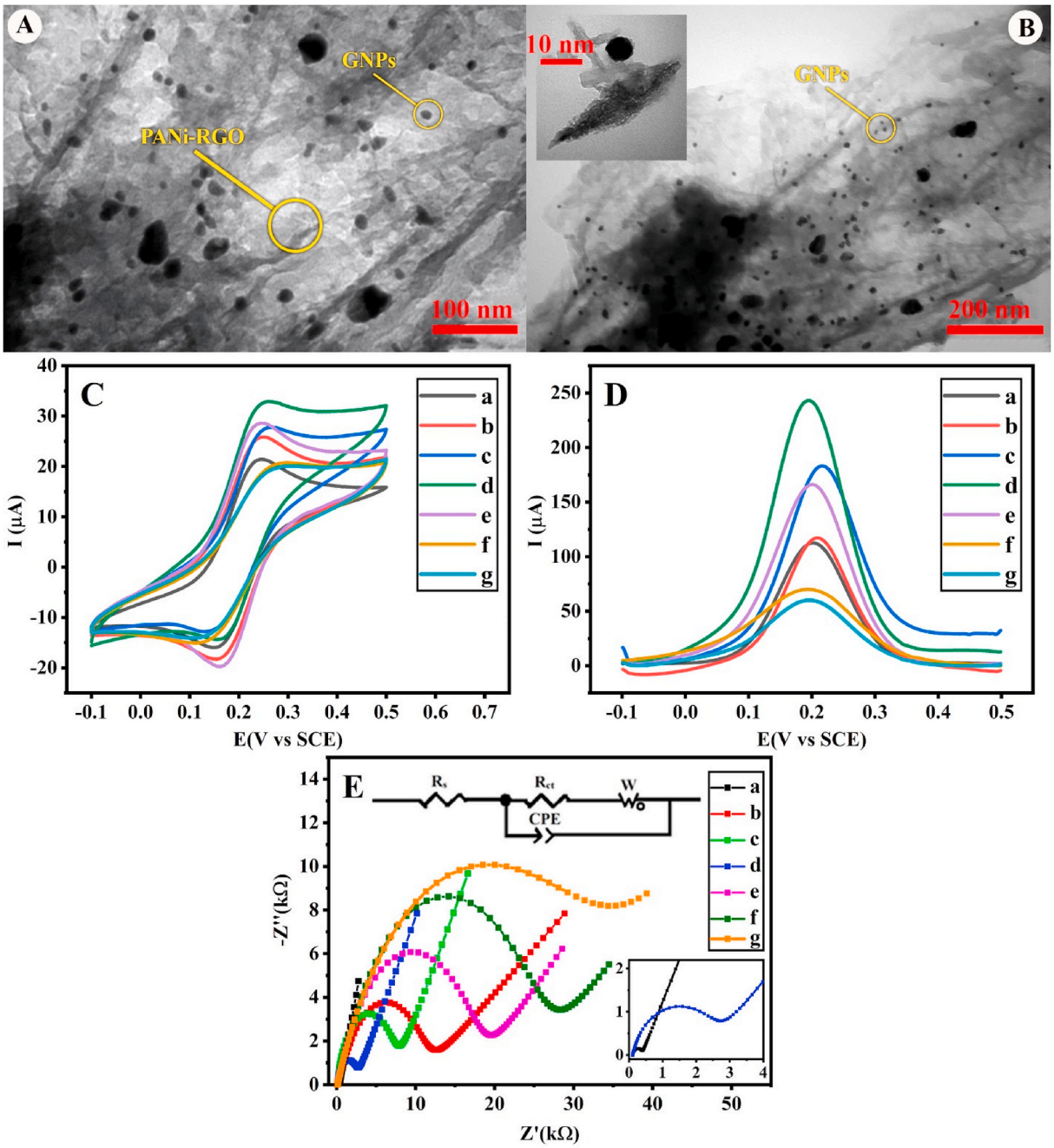

Fig. 1. (A and B), TEM images of PANi–RGO–G*NPs nanocomposite 100 nm and 200 nm scale, inset:10 nm scale), (C) CV, (D) SWV and (E) EIS experiments conducted from 10 mHz to 100 kHz at 0.215 V for (a) bare Au, (b) PANi–RGO/Au, (c) PANi–RGO–GNPs/Au, (d) PANi–RGO–G*NPs/Au, (e) Apt/PANi–RGO–G*NPs/Au, (f) BSA/Apt/PANi–RGO–G*NPs/Au, and (g) TApt/PANi–RGO–G*NPs/Au electrodes recorded at pH 7.4 in B-R buffer containing 5 mM $Fe[(CN)_6]^{3-/4-}$, 0.3 M KCl, and 20 mM NaCl. In the inset (Fig. 1 E) is reported the equivalent circuit diagram for the TApt/PANi–RGO–G*NPs/Au electrode.

methylene blue (Dong et al., 2020). Although these technologies afford increased sensitivity of the biosensor, these compounds are usually toxic and expensive, and their use involves laborious and complicated preparation procedures (Huang et al., 2017). Conventional electrodes, such as Pt, Au, and graphite, are characterized by a poor electrochemical behavior, a narrow linear range, and high over-potential electrochemical oxidation with DNA (Kim et al., 2007). However, researchers have found a way to solve these problems by using new materials to modify electrodes. New sciences have been developed following various nanoscale electrochemical measurements to improve performance, such as nanostructures, nanoparticles, and nanotubes, and they have been used to build nanosensors (Shi et al., 2014) by using nanomaterials (Chen et al., 2015). Therefore, researchers are looking to build a label-free E-DNA biosensor based on direct electron transfer to produce a simple, economical, and green such biosensor. Conducting polymers CP, reduced graphene oxide (RGO), nanoparticles (NPs) and CP/NPs composites are some of the most promising categories of materials in terms of the design of E-DNA biosensors (Sun et al., 2012). Polyaniline (PANi) and PANi/NPs composites have been widely used to construct novel electrochemical biosensors(Shi et al., 2014). Gold nanoparticles (GNPs), with specific electrical properties, are among the best candidates for electrical devices. One of the strategies to improve the electrical properties of GNPs is the preparation of their composites with RGO (Niu et al., 2017).

In the present study, the doping of RGO with PANi and GNPs was investigated as a strategy to improve RGO performance as electrode material for E-DNA biosensors. For this propose, the DYS14 aptamer/polyaniline–reduced graphene oxide–gold nanoparticles/gold (Apt/PANi–RGO–G*NPs/Au) electrode was fabricated electrochemically. In order to achieve the modification of the oligonucleotides of the DYS14 aptamer, the non-bridging oxygen atom on the phosphate backbone was replaced with a sulfur atom, so as to form a phosphorothioate linkage. This method of oligonucleotide modification is cheaper and simpler to implement than SH-modification (Zhou et al., 2014). Importantly, we also used a tandem phosphorothioate PS-modified ssDNA for the attachment of ssDNA to GNPs. In order to easily immobilize, 29 bases oligonucleotides were selected as E-DNA biosensor probes. The new Apt-PANi–RGO–G*NPs/Au) electrode was fabricated and used for the early determination of fetal gender using cffDNA, introducing an approach that can be considered as a non-invasive pre-test.

2. Experimental

2.1. Materials and apparatus

All organic solvents and raw materials, including aniline (99%), $K_3[Fe(CN)_6]$, $K_4[Fe(CN)_6]$, graphite powder, $HAuCl_4{\cdot}3H_2O$, and bovine serum albumin (BSA), were purchased from Sigma-Aldrich or Merck in analytical grade and used without further purification. The DNP^{TM} Kit DNA extraction solution (Sinacolon Co., Iran) and Taq DNA polymerase 2X Master Mix RED were purchased from Ampliqon/Biomol (Denmark) and used as purchased. Sterilized double-distilled water (SDDW) was used for the preparation of stock solutions. The Britton–Robinson (B–R) buffer 0.04 M (pH 7.4 and 4.8) was utilized as a supporting electrolyte. All the oligonucleotides related to the DYS14 gene were supplied from BIONEER Co., South Korea, and they had the sequences specified as follows. The DNA probe (29-mer base sequence: 5′-CTTCGTCAGTGATCAGGGCTAAAAAAA*A*A-3′) was designed using the Allel ID software, and it was received as a lyophilized powder. The target DNA (20-mer base sequence: 5′-AGCCCTGATCACTGACGAAG-3′), aptamer specificity, and DYS14 gene were checked by the National Center for Biotechnology Information (NCBI). All oligonucleotides were dissolved in 10.0 mM Tris-HCl and 1.0 mM EDTA at pH 7.4 (TE buffer), and the resulting solutions were kept frozen. The clinical plasma samples were prepared by a pathology laboratory. DNA hybridization was carried out at 56 °C whereas the electrochemical experiments were performed at ambient temperature. All experiments were carried out in electrochemical cells, and pure nitrogen gas was used to deoxygenate sample solutions before each experiment. Details of experimental apparatus can be found in Supporting Information (SI).

2.2. Blood sampling, DNA extraction, PCR and preparation of PANi–RGO–G*NPs/Au electrodes and the DYS14 E-DNA biosensor

All steps for sample preparation and PCR were performed following literature protocols (Moradi et al., 2019). More details for blood sampling, DNA extraction, PCR and preparation of PANi–RGO–G*NPs/Au electrodes and the DYS14 E-DNA biosensor can be found in SI. An illustration of the PANi–RGO–G*NPs/Au electrode preparation and proposed E-DNA biosensor fabrication process is depicted in Scheme 1. The modified Hummer method was implemented as reference for the synthesis of graphene oxide (GO) (Badia et al., 1997). Details of GO preparation can be found in SI. The produced GO was characterized by XRD and FT–IR. CVs of bare gold electrode, growth of PANi-RGO and PANi-RGO-GNPs nanocomposites on the surface of clean gold electrode are shown in Fig. S1 explained in Supporting Information (SI).

3. Results and discussion

3.1. DNA purity and PCR characterization

In order to check the quality of the extracted genomic DNA, all extracted genomic DNA samples from ten healthy and fertile men were run on agarose gel (1% agarose) by electrophoresis. Between the samples, only four genomic DNA has good qualities for PCR (Fig. S2A). However, sample number 4 proved to be the best one, and this sample was selected to be used in the rest of the study. In order to choose the annealing temperature of the PCR experiment, a gradient manner temperature of 54–56 °C (Fig. S2B) was adjusted on sample 4. After running the PCR products on agarose gel electrophoresis (1% agarose), 56 °C was chosen as the optimum annealing temperature for the PCR program.

3.2. Characterization of PANi–RGO–GNPs/Au electrodes and DYS14 E-DNA biosensor

The FT–IR spectra of GO, RGO, PANi, PANi–RGO, PANi–RGO–G*NPs, and Apt/PANi–RGO–G*NPs in the 500–4000 cm^{-1} range are reported in Fig. S3. The major bands and their assignments for GO, RGO, PANi, and PANi–RGO (Figs. S3a–d) are in good agreement with their counterparts reported in other published studies (Gandara and Gonçalves, 2020). The FT–IR spectrum of PANi–RGO–G*NPs (Fig. S3e) and Apt/PANi–RGO–G*NPs (Fig. S3f) confirm the immobilization of the DYS14 aptamer on the surface of PANi–RGO–G*NPs. More details of FT-IR characteristic bands of the samples are available in SI. The SEM images of the synthesized materials, pure RGO, PANi, PANi–RGO, PANi–RGO–GNPs, PANi–RGO–G*NPs, Apt/PANi–RGO–G*NPs, Apt/PANi–RGO–G*NPs covered by BSA, and target sequence on Apt/PANi–RGO–G*NPs covered by BSA are reported in Figs. S4 and S5. More details of SEM analysis are available in SI. The presence in the PANi–RGO–G*NPs nanocomposite of GNPs with diameters in the 10–20 nm range was confirmed by TEM evidence (Fig. 1A and B). These GNPs in the three-dimensional structure of the nanocomposite cause it to display improved conductivity with respect to PANi–RGO, rendering PANi–RGO–G*NPs a good candidate for the construction of an E-DNA biosensor. Indeed, TEM evidence indicates that the RGO sheets were covered by GNPs and PANi. Notably, RGO has several oxygen functional groups, which can provide a large number of active sites for trapping the aniline oligomer, leading to the formation of PANi nuclei. During the growth step of the PANi–RGO–G*NPs nanocomposite, GNPs were captured by PANi.

The results of (EDX) analyses performed on PANi–RGO–G*NPs and Apt/PANi–RGO–G*NPs are reported in Fig. S6. The spectra of PANi–RGO–G*NPs (Fig. S6A) confirm the presence of C, N, O, and Au atoms in the nanocomposite. Moreover, the spectrum of Apt/PANi–RGO–G*NPs (Fig. S6B) confirms the presence of C, N, O, P, S, and Au atoms. The decreasing weight of C, N, O, and Au atoms and the appearance of new peaks due to P and S are indicative of the successful synthesis of Apt/PANi–RGO–G*NPs.

The XRD pattern of the obtained GO powder, RGO powder, bare Au electrode, PANi, PANi–RGO, and PANi–RGO–G*NPs nanocomposite on the Au electrode are reported in Fig. S7. Details of XRD for the samples are available in SI.

3.3. Electrochemical measurements

The successful modification of the fabricated biosensor (Apt/PANi–RGO–G*NPs/Au) was checked by CV and SWV utilizing a 5 ml of 0.04 M B–R buffer solution (pH 7.4) containing $[Fe(CN)_6]^{3-/4-}$ (redox probe) 5 mM. The obtained results are presented in Fig. 1C and D. By modifying of the bare gold electrode (Fig. 1C–a) with PANi–RGO, an increase in the peak current of the cyclic voltammogram was observed (Fig. 1C–b). This observation can be due to an increase in the number of electrochemically active sites. The graphene sheet provides a suitable substrate for

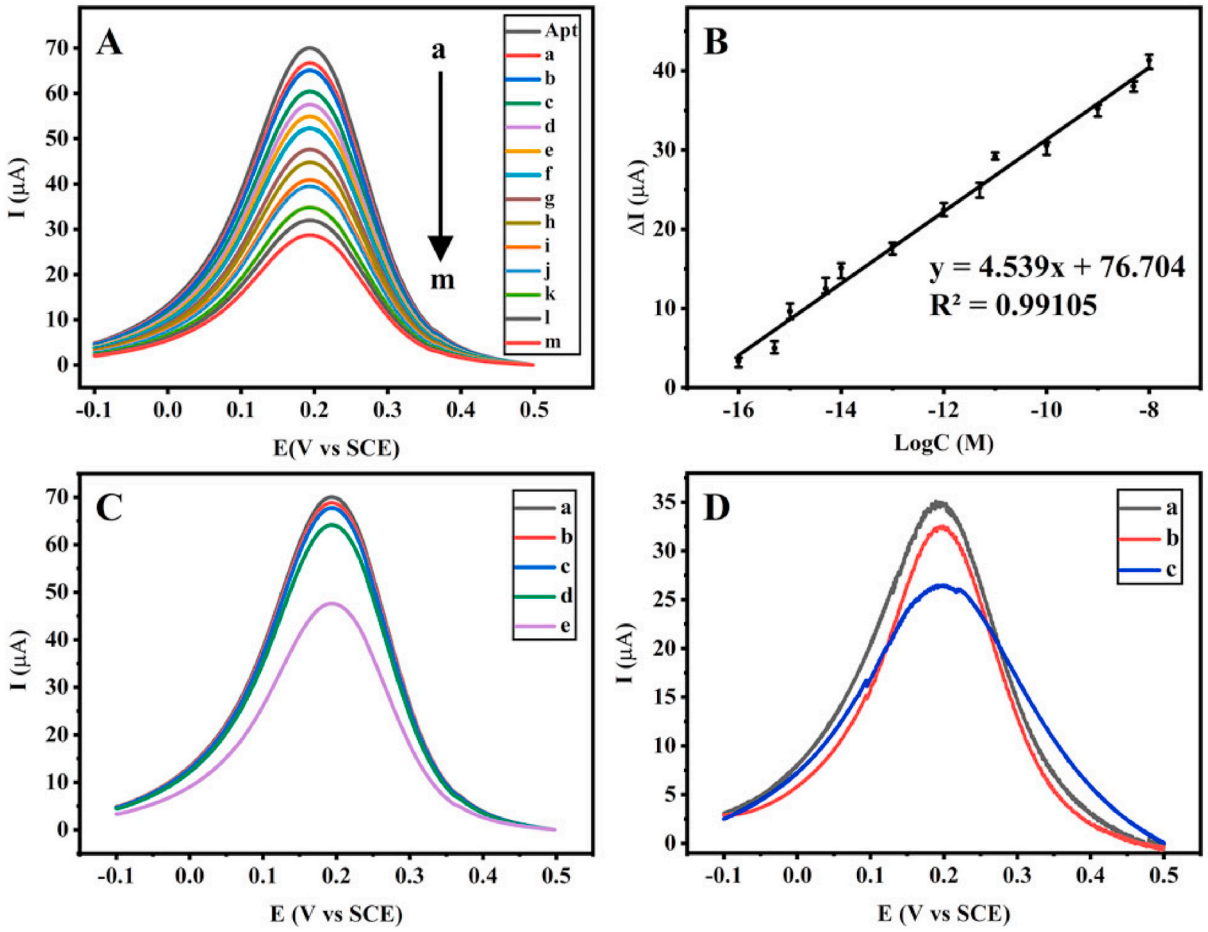

Fig. 2. (A) SWV profiles of the TApt/PANi–RGO–G*NPs/Au electrode in different concentrations of the complementary DNA sequence (curves from a to m): 1×10^{-16}, 5×10^{-16}, 1×10^{-15}, 5×10^{-15}, 1×10^{-14}, 1×10^{-13}, 1×10^{-12}, 5×10^{-12}, 1×10^{-11}, 1×10^{-10}, 1×10^{-9}, 5×10^{-9}, and 1×10^{-8} M in blank solution (0.04 M B-R buffer (pH 7.4) containing KCl 0.3 M, NaCl 20 mM, and $[Fe(CN)_6]^{3-/4-}$ 5 mM), (B) calibration plot of the relative change in SWV peak current of the proposed TApt/PANi–RGO–G*NPs/Au electrode versus the logarithm of the concentration of the complementary DNA sequence under optimized experimental conditions and RSD 2.4%, (C) SWVs of the (a) Apt/PANi-RGO-G*NPs/Au electrode without target sequence and (b) with noncomplementary DNA, (c) the four base mismatch DNA (d) the one base mismatch DNA and (e) the complementary DNA in blank solution, under the optimal conditions and anodically scanning the electrode potential between -0.10 and 0.50 V and (D) SWV of the TApt/PANi–RGO–G*NPs/Au electrode immersed in solutions of the polymerase chain reaction product of the DNA target sequence at different concentrations (sample a: 3.30×10^{-9} M; sample b: 6.60×10^{-9} M; sample c: 1.23×10^{-8} M) in blank solution.

the *in-situ* electro-polymerization of aniline and the formation of PANi–RGO on the gold surface. The oxidation peak potential of the modified electrode shifted to more positive values with respect to the bare electrode, which indicates that the electronic transfers were more difficult at the surface of the PANi–RGO/Au electrode than at that of the bare gold electrode.

By performing a double electrodeposition of GNPs on the surface of the PANi–RGO–GNPs/Au electrode, the peak current position and peak potential of the modified PANi–RGO–G*NPs/Au electrode increased and shifted to lower potential values, respectively (Fig. 1C and d). These observations are due to an increase in the amount of GNPs, an expansion of the area of the active surface, and an improvement of the conductivity of the electrode. In other words, the electrode performance and activity of the cover increased as a result of the double electrodeposition of GNPs. The GNPs in the polymer nanocomposite matrix can act as connectors between the aptamer and the electrode's surface, leading to the uniform dispersion of DNA probes, and the signal of the E-DNA biosensor has become more assertive. In the case of the Apt/PANi–RGO–G*NPs/Au electrode (Fig. 1C–e), the intensity of the current decreased, and the oxidation peak potential shifted to more positive values. These observations are due to the sufficient binding of aptamer and the limits electron transfer on the surface of GNPs. The same trends were observed for the BSA/Apt/PANi–RGO–G*NPs/Au electrode (Fig. 1C–f). By immersing the Apt/PANi–RGO–G*NPs/Au electrode in BSA solution, the other active sites available for the interaction with $[Fe(CN)_6]^{3-/4-}$ were covered. By placing the Apt/PANi–RGO–G*NPs/Au electrode in the solution containing the target DNA sequence, the electrode dubbed TApt/PANi–RGO–G*NPs/Au (Fig. 1C–g) was constructed, for which a reduced current value was observed. These definite and repeatable voltammogram (Fig. 1C–g) indicates a stable aptamer connection and complete BSA coverage of the electrode.

The results of the implementation of the SWV technique are reported in Fig. 1D. Changes in current intensities and shifts in oxidation potential of the peak were observed. Using the PANi–RGO–G*NPs/Au electrode, the oxidation peak potential of $[Fe(CN)_6]^{3-/4-}$ shifted in the negative direction with respect to the PANi–RGO/Au electrode. These changes in peak current and potential can be due to synergistic effects among RGO, PANi, and GNPs whereby electron transfer becomes facilitated and the effective surface area of the electrode increases. The mechanism of electron exchange between the $[Fe(CN)_6]^{3-/4-}$ and Apt/PANi–RGO–G*NPs/Au electrode process can be study by Randles-Sevich equation (Bard and Faulkner, 2001). The electrons flow from the electrode surface to RGO-PANi-G*NPs nanocomposites, then, the electrons were transfer by P–S bond from gold nanoparticles to the aptamer and redox probe. Based on the Randles-Sevich equation, the CVs of $[Fe(CN)_6]^{3-/4-}$ (Fig. S8) at different scan rates on modified electrodes

increased linearly with square root of scan rate in $[Fe(CN)_6]^{3-/4-}$ 5 mM which indicated that the electrochemical reaction is under a diffusion control process. The slop of the plot of reduction peak current of $[Fe(CN)_6]^{3-/4-}$ against square root of scan rate and effective surface area values of the modified electrodes were calculated and reported in Table S1.

EIS is a powerful technique to investigate the interface between the surfaces of the Au, PANi–RGO/Au, PANi–RGO–GNPs/Au, PANi–RGO–G*NPs/Au, Apt/PANi–RGO–G*NPs/Au, BSA/Apt/PANi–RGO–G*NPs/Au, and TApt/PANi–RGO–G*NPs/Au electrodes and the solutions in which they are immersed. In particular, EIS experiments were conducted with the said electrodes immersed in solutions containing the B–R buffer (0.04 M, pH 7.4), $[Fe(CN)_6]^{3-/4-}$ 3.0 mM, and KCl 0.3 M at 0.215 V with a frequency range of 10 mHz to 100 kHz, and the results thus obtained are reported in Fig. 1E. The values of the semicircular diameters in the high-frequency region provide information on the charge transfer resistance (R_{ct}) that controls the charge transfer and on the kinetics of the interface oxidation probe at the electrode interface. The bare gold electrode (curve a) retail is 263 Ω and shows an excellent electron transfer advantage from the proposed method.

The EIS curve of the modified PANi–RGO–G*NPs/Au electrode (curve (d)) is almost a straight line. By performing a double electrodeposition of GNPs on the surface of the PANi–RGO–GNPs/Au electrode, the number of gold nanoparticles on the surface of the electrode increased, so that the electrode's electrical conductivity increased and the value of R_{ct} decreased significantly. Notably, these observations are due to the increase in the number of gold nanoparticles in the PANi–RGO–G*NPs matrix. After immobilization of the aptamer probes, the R_{ct} value of Apt/PANi–RGO–G*NPs/Au electrode (curve e) increased with respect to its PANi–RGO–G*NPs/Au precursor to 23.906 kΩ. This change is due to the assembly of the backbone of the negatively charged phosphoric acid DNA probe, which prevents electron transfer. After sealing the electrodes with BSA and target DNA sequence (curves (f) and (g), respectively), the R_{ct} values increased to 28.412 kΩ and 31.286 kΩ, respectively. These observations descend from the blockage of the hybrid with target DNA and target aptamer formations. The increase in R_{ct} value is also due to the large amount of negative charges in the phosphoric acid backbone of the aptamer, and a combination of the DNA with the electrode surface. Additionally, when the complement DNA sequence is attached to the electrode, the R_{ct} value increases significantly.

The values of the elements in equivalent circuits of Fig. 1E fitted in the Nyquist diagrams are listed in Table S2. These observations confirm the binding of the complement sequence to the electrode surface, resulting in the successful fabrication of the TApt/PANi–RGO–G*NPs/Au electrode (Sypabekova et al., 2019). Notably, the equivalent circuit diagram for the TApt/PANi–RGO–G*NPs/Au electrode is reported in the inset of Fig. 1E.

3.4. Optimization of pH, experimental variables, and instrumental parameters

In order to achieve the best chemical and electrochemical results and maximum performances of the fabricated Apt/PANi–RGO–G*NPs/Au electrode, G*NPs deposition time, buffer solution selection, pH, probe concentration, probe immobilization time, and hybridization time were evaluated and optimized. The obtained optimized values were 150 s, 5 × 10^{-10} M, 10 and 5 min, respectively (Fig. S9). In order to optimize the instrumental parameters of the prepared E-DNA biosensor, repeatability and reproducibility were investigated in B–R buffer (pH 7.4) containing 1 × 10^{-13} and 1 × 10^{-9} M of the complementary sequence. The optimized values for these parameters are listed in Table S3. More details about optimization is available in SI.

3.5. Hybridization and electrochemical detection

The electrochemical behavior of the E-DNA biosensor was investigated by SWV by immersing the TApt/PANi–RGO–G*NPs/Au electrode in 5 ml of 0.04 M B–R buffer (pH 7.4) containing KCl 0.3 M, NaCl 20 mM, and $[Fe(CN)_6]^{3-/4-}$ 5 mM, and anodically scanning the electrode potential between −0.10 and 0.50 V (Fig. 2A). The assay time was 30 s. The same protocol was implemented in the case of the Apt/PANi–RGO–G*NPs/Au electrode following hybridization of the probe with complementary or non-complementary DYS14 DNA sequences. Notably, as the concentration of the complementary DNA sequence increased, the intensity of the current peaks decreased (curves a–m in Fig. 2A), tandemly.

This observation descends from the connection of the target sequence to the E-DNA biosensor and the occupation of the electron transfer site. The calibration plot of the relative change in the peak currents of SWV of the proposed TApt/PANi–RGO–G*NPs/Au electrode under the optimal conditions with different concentrations of the complementary DNA sequence are reported in Fig. 2B. A linear relationship was observed to exist between the decrease in the intensity of the peak currents and the values of the logarithm of the concentration of the complementary DNA sequence in the 1 × 10^{-16}–1 × 10^{-8} M range. The regression equation thus obtained could be expressed as y = 4.539log C + 76.704, with a value for the correlation coefficient (R^2) of 0.99105. In optimize conditions (see section 3.4, Fig. S9 and Table S3), the detection limit (LOD) and limit of quantitation (LOQ) of the target DNA sequence were estimated to be 3S/N = 4.26 × 10^{-17} M and 10S/N = 1.422 × 10^{-16} M, respectively. Using limit of blank (LoB), standard deviation (SD), mean result, LoB = mean $_{blank}$ + 1.645(SD $_{blank}$) formula and LOD = LoB + 1.645(SD $_{low\ concentration\ sample}$ formula, the limit of detection is calculated to be 4.55 × 10^{-17} M (Armbruster and Pry, 2008), which is in good agreements with LOD from 3S/N formula. The regeneration process of E-DNA sensor was carried out by denaturation of complementary DNA modified Apt/PANi–RGO–G*NPs/Au (Fig. S10A). The regenerated of modified electrode could maintain with high activity for around 95.80% of its response after 4 times regenerating and RSD about 2.70% (n = 3). The stability of the E-DNA sensor in a B-R buffer for 3 weeks was investigated (Fig. S10B). The sensor was kept in 4 °C in 10 mM Tris-buffer (pH 7.4). It was found that the fabricated E-DNA sensor 95.01% with RSD; 2.96%, n = 3 of the original signal indicating good life time and stability.

In order to investigate the selectivity of the fabricated E-DNA biosensor, a sample without target sequence (sample a, in blank solution consisting of B–R buffer containing KCl 0.3 M, NaCl 20 mM,and $[Fe(CN)_6]^{3-/4-}$ 5 mM) was evaluated under the optimal conditions. Additionally, four samples containing as many different kinds of target sequences were also evaluated; these target sequences included non-complementary DNA (sample b), a DNA sequence with four-base-mismatch with respect to complementary DNA (sample c), a one-base mismatch DNA sample (sample d), and complementary DNA (sample e). The SWV curves of the described samples are reported in Fig. 2C.

The aptamer current measured in the blank solution (curve a) had a value of ~70 μA. This current is nearly as high as that measured in non-complementary DNA solution. Among the solutions containing the four DNA sequences, the current measured in the complementary DNA solution (curve e) had a much lower value than those of the other solutions containing target DNA sequences (curves b–d). These SWV responses demonstrated that the fabricated E-DNA biosensor was characterized by high selectivity and sensitivity in the detection of the complementary DNA sequence. The analytical properties of the proposed Apt/PANi–RGO–G*NPs/Au E-DNA biosensor were compared to those of other sensors (Table S4). The fabricated E-DNA biosensor displayed superior performance to other reported biosensors, in terms of either the size of the linear range or the value of the limit of detection.

Identification and quantification of DYS14 PCR product sequence and cffDNA in actual biological samples SWV experiments were

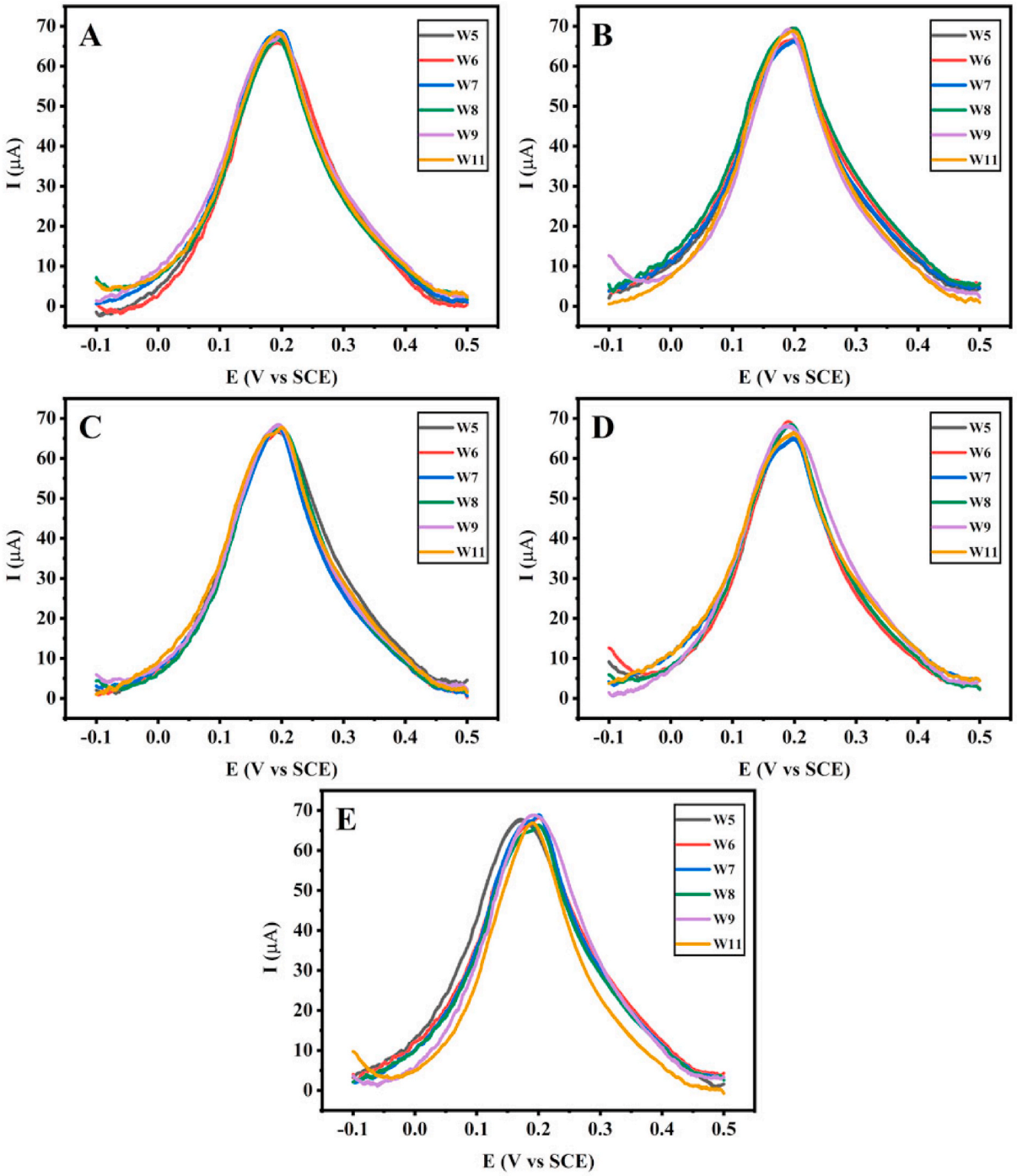

Fig. 3. SWV obtained using the TApt/PANi–RGO–G*NPs/Au electrode in different diluted maternal blood plasma samples of cffDNA (collected from 5 women samples A–E) diluted in 0.04 M of B-R buffer (pH 7.4) containing KCl 0.3 M, NaCl 20 mM, and $[Fe(CN)_6]^{3-/4-}$ 5 mM. The voltammograms were recorded under optimized conditions, and the electrode potential was anodically scanned between −0.10 and 0.50 V W5–W11: week 5 of gestation–week 11 of gestation.

conducted to identify and quantify the PCR product of DNA target solutions at various concentrations using the TApt/PANi–RGO–G*NPs/Au electrode in B–R buffer 0.04 M (pH 7.4) containing KCl 0.3 M, NaCl 20 mM, and $[Fe(CN)_6]^{3-/4-}$ 5 mM. The obtained data are reported in Fig. 2D. The Apt/PANi–RGO–G*NPs/Au E-DNA biosensor was combined with the products of the application of PCR technology to measure the amount of DYS14 sequence present in real Y chromosomes extracted from men's blood. Indeed, the template was amplified by PCR, the annealing temperature of the procedure was optimized, and the highest-purity product of a single molecule was obtained.

In order to determine the purity of the sample, the ratio of UV absorption intensity at two wavelengths, 260 and 280 nm, of the PCR amplification sample was calculated, and the obtained value for A260/A280 was 1.84, indicating the high purity of the analyte (Raimundo et al., 2018). The purified PCR sample (1 μl) was diluted with 5 ml of 0.04 M B–R buffer (pH 7.4), denatured by being subjected to heating at 92 °C in water for 5 min, and then cooled to 56 °C. After the immobilization of the DYS14 sequence probe on the Apt/PANi–RGO–G*NPs/Au electrode, the constructed electrode was immersed in 5 mL of denatured PCR amplification product to hybridize the aptamer under optimal conditions. Based on SWV evidence, the current value decreased slightly as the PCR product's concentration increased from 3.30×10^{-9} to 1.23

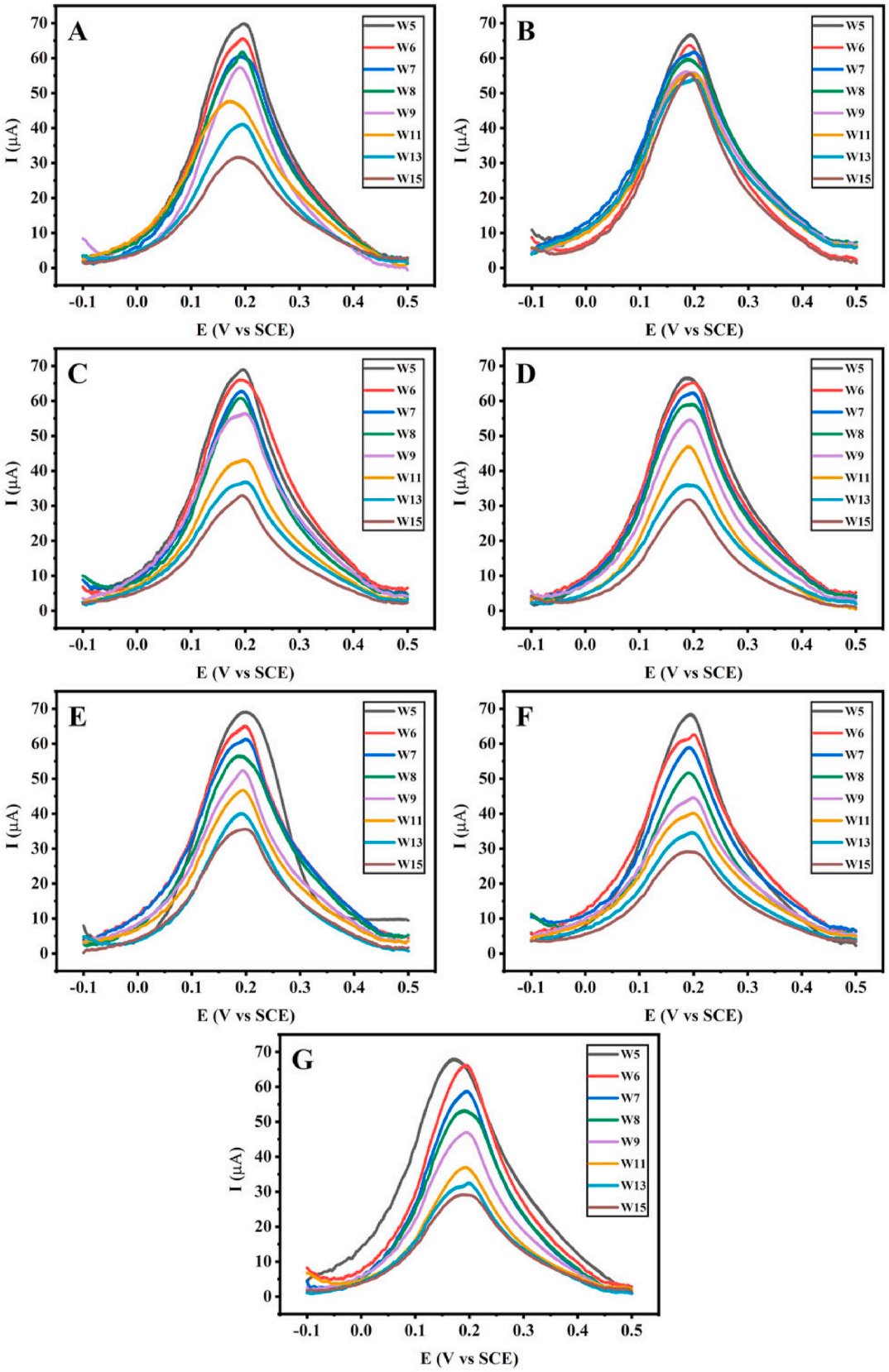

Fig. 4. SWV obtained using the TApt/PANi–RGO–G*NPs/Au electrode in different diluted maternal blood plasma samples of cffDNA (collected from 7 women -samples A–G) diluted in 0.04 M of B-R buffer (pH 7.4) containing KCl 0.3 M, NaCl 20 mM, and $[Fe(CN)_6]^{3-/4-}$ 5 mM. The voltammograms were recorded under optimized conditions, and the electrode potential was anodically scanned between −0.10 and 0.50 V W5–W15: week 5 of gestation–week 15 of gestation.

Table 1
Maximum peak current values inferred from Figs. 3 and 4 for blood plasma samples collected from 12 selected pregnant women from the 5th to the 15th week of pregnancy. (F: female sex of the fetus; M: male sex of the fetus).

Week of pregnancy	Maximum current values (μA) inferred from the data in Figs. 3 and 4											
	3A (F)	3B (F)	3C (F)	3D (F)	3E (F)	4A (M)	4B (M)	4C (M)	4D (M)	4E (M)	4F (M)	4G (M)
5th	69.19	69.32	68.75	68.09	67.46	69.13	68.19	69.34	68.54	69.92	69.45	69.65
6th	67.11	68.91	67.16	69.92	68.21	66.05	65.06	67.13	65.56	66.61	62.39	67.14
7th	69.85	67.31	69.03	66.84	69.47	61.14	63.18	64.37	63.52	62.64	60.18	59.89
8th	68.27	69.28	67.89	69.34	67.21	60.35	61.62	61.53	60.55	58.14	52.24	54.65
9th	67.41	69.26	69.82	69.74	69.62	57.38	59.74	57.75	56.14	53.03	46.52	47.66
11th	69.82	67.92	67.76	68.25	67.11	46.79	58.18	44.23	48.78	47.07	41.64	37.87
13th	–	–	–	–	–	39.98	55.68	37.61	37.01	41.12	35.46	32.98
15th	–	–	–	–	–	32.06	57.55	33.27	32.37	36.15	30.61	30.53

$\times 10^{-8}$ M. This observation is due to the binding of the PCR products (DYS14 sequence) to the aptamer. The data collected for PCR products characterized by various concentrations of the DNA target solutions are listed in Table S4. For selected concentrations of the said PCR products (samples a–c), the differences in value between the I_t current for TApt/PANi–RGO–G*NPs/Au and the I_{ap} aptamer current for Apt/PANi–RGO–G*NPs/Au ($\Delta I = I_t - I_{ap}$.) for the PCR product of the DNA sequence target were calculated and fitted to the calibration curve reported in Fig. 2B. The results thus obtained indicate that the current differences (ΔI) matched the logarithmic concentrations of the proposed TApt/PANi–RGO–G*NPs/Au electrode.

The SWV measurements corroborated the idea that the Apt/PANi–RGO–G*NPs/Au electrode could be utilized to successfully recognize and detect the PCR amplification products of the DYS14 sequence in actual Y-chromosome samples.

In order to evaluate the performance of the E-DNA biosensor in real samples, the blood plasma samples of 12 selected pregnant women were collected to determine the sex of the fetus. SWV experiments were conducted under optimal conditions using the TApt/PANi–RGO–G*NPs/Au electrode for the detection and quantification of cffDNA in diluted plasma samples obtained from maternal blood; the results of these experiments are reported in Figs. 3 and 4. All plasma samples were prepared in the pathology laboratory and diluted with hybridization buffer (10.0%, v/v) due to elimination of matrix effects (Rosenberg-Hasson et al., 2014), denatured by heating in water bath at 92 °C for 5 min, and then cooled in a 56 °C bath. The Apt/PANi–RGO–G*NPs/Au electrode was immersed in 5 ml of the prepared denatured DNA sample to allow its hybridization with the aptamer under optimal conditions. Additionally, in order to reduce the diagnostic error in determining the sex of the fetus, all experiments were performed with three precisely the same E-DNA biosensor and under the same conditions. The ccollection of blood samples form pregnant women started in the 5th week of pregnancy. By the end of the 7th week, the response of the E-DNA biosensor to the presence of chromosomes Y in the samples indicated the possibility of the male sex of the fetus. To confirm the sex determination thus made, the experiments were continued until the end of the 11th week of pregnancy. As can be evinced from the E-DNA biosensor response measured in five samples (Fig. 3A–E), the maximum currents did not change in value during measurements and remained in the 67–70 μA range. This observation indicated the absence of Y chromosomes in the blood plasma of the relevant pregnant women; therefore, the sex of the fetus was concluded to be female.

In the case of the other seven samples (Fig. 4A–G), the E-DNA biosensor response was characterized by a decrease in current intensity up to the 15th week of pregnancy from 70 to 30 μA; the sex of the fetus was thus evinced to be male. The maximum current values observed for the 12 selected pregnant women's blood plasma samples collected from the 5th to the 15th week of pregnancy are listed in Table 1. The results of 12 selected pregnant women's blood plasma show that the 41.66% of the samples are female and 58.34% are male, which is in good agreement with the data obtained from the PCR method. The data reported for actual plasma samples suggest that use of the proposed Apt/PANi–RGO–G*NPs/Au E-DNA biosensor is appropriate for the efficient detection of the DYS14 DNA sequence, so that this E-DNA biosensor can be used to determine fetal sex in pregnant women between the 7th and 9th week of pregnancy. The purpose of the fabricated sensor is to eliminate the PCR process due to high cost and time. In addition, in the screening process and in healthcare, the use of present sensor reduces time and cost.

4. Conclusions

The Apt/PANi–RGO–G*NPs/Au electrode was fabricated electrochemically, and its use proved successful in the determination of the fetus sex via analysis of pregnant women blood plasma between the 7th and 9th week of pregnancy. The E-DNA biosensor was shown high selectivity and sensitivity, high efficiency, and acceptable repeatability. Under optimal conditions, the LOD and LOQ of the propose biosensor had values of 4.26×10^{-17} and 1.422×10^{-16} M, respectively. The results demonstrate that the fabricated biosensor can be used for the efficient detection of the DYS14 DNA sequence in the Y-chromosome. We hope that the proposed analytical method can be used as a model for the investigation of viruses or bacteria genome.

CRediT authorship contribution statement

Mahdi Malmir: Designed and performed experiments, analyses data and writing. **Jalal Arjomandi:** Corresponding author, Supervision, Conceptualization, Methodology, reviewing and editing. **Abolfazl Ghafouri Khosroshahi:** Consultant and project guide assistance. **Mohammadreza Moradi:** Performed experiments, consultant and project guide assistance. **Hu Shi:** Co-wrote the paper, editing, instrumental supports.

Declaration of competing interest

The authors declare the following financial interests/personal relationships which may be considered as potential competing interests: The authors of this manuscript receives research support from (1) Bu Ali Sina University (Hamedan, Iran), (2) University of Sciences, (Hamedan, Iran), and (3) Shanxi University (Taiyuan, China).Written informed consent was obtained from each participant before collecting blood. Ethical approval was obtained from the Ethics Committee of the Bu Ali Sina Univesrsity, Hamedan, (Ir. BASU.REC.1398.033).Fully edited the text has been done by ",; enago Editing Service" LUIJBC-1381, Jan. 14, 2021.

Acknowledgment

We would like to thank Hamadan University of Pharmacy and Medical Sciences for providing the necessary conditions for the experiments and Dr. Mousavi Pathobiology Laboratory in Razan for providing and maintaining laboratory samples.

Appendix A. Supplementary data

Supplementary data to this article can be found online at https://doi.org/10.1016/j.bios.2021.113356.

References

Armbruster, D.A., Pry, T., 2008. Clin. Biochem. Rev. 29, S49.
Badia, A., Cuccia, L., Demers, L., Morin, F., Lennox, R.B., 1997. J. Am. Chem. Soc. 119, 2682–2692.
Bard, A.J., Faulkner, L.R., 2001. Methods 2, 580–632.
Chen, X., Wang, Q., Wang, L., Guo, H., Yang, Y., Li, F., Gao, F., 2015. Ind. Eng. Chem. Res. 54, 1520–1528.
Dong, Y., Yao, C., Zhu, Y., Yang, L., Luo, D., Yang, D., 2020. Chem. Rev. 120, 9420–9481.
Gandara, M., Gonçalves, E.S., 2020. Prog. Org. Coating 138, 105399.
Huang, Q., Lin, X., Zhu, J.-J., Tong, Q.-X., 2017. Biosens. Bioelectron. 94, 507–512.
Karastogianni, S., Girousi, S., 2015. Chem. Pap. 69, 202–210.
Kim, Y.S., Jung, H.S., Matsuura, T., Lee, H.Y., Kawai, T., Gu, M.B., 2007. Biosens. Bioelectron. 22, 2525–2531.
Lun, F.M.F., Chiu, R.W.K., Allen Chan, K.C., Yeung Leung, T., Kin Lau, T., Dennis Lo, Y. M., 2008. Clin. Chem. 54, 1664–1672.
Moradi, M., Saidijam, M., Ghaleiha, A., Jahangard, L., Yadegarazari, R., Keshavarzi, A., 2019. Neurochem. J. 13, 210–214.
Niu, X., Zheng, W., Yin, C., Weng, W., Li, G., Sun, W., Men, Y., 2017. J. Electroanal. Chem. 806, 116–122.
Odeh, F., Nsairat, H., Alshaer, W., Ismail, M.A., Esawi, E., Qaqish, B., Bawab, A. Al, Ismail, S.I., 2020. Molecules 25, 3.
Radhakrishnan, S., Sumathi, C., Dharuman, V., Wilson, J., 2013. Anal. Methods 5, 1010–1015.
Raimundo, J., Reis, C.M.G., Ribeiro, M.M., 2018. Mol. Biol. Rep. 45, 1405–1412.
Rosenberg-Hasson, Y., Hansmann, L., Liedtke, M., Herschmann, I., Maecker, H.T., 2014. Immunol. Res. 58, 224–233.
Shi, A., Wang, J., Han, X., Fang, X., Zhang, Y., 2014. Sensor. Actuator. B Chem. 200, 206–212.
Su, X., Wu, Y.-J., Knoll, W., 2005. Biosens. Bioelectron. 21, 719–726.
Sun, W., Qi, X., Zhang, Y., Yang, H., Gao, H., Chen, Y., Sun, Z., 2012. Electrochim. Acta 85, 145–151.
Sun, W., Song, W., Guo, X., Wang, Z., 2017. Anal. Chim. Acta 978, 42–47.
Sypabekova, M., Dukenbayev, K., Tsepke, A., Akisheva, A., Oralbayev, N., Kanayeva, D., 2019. Sci. Rep. 9, 1–11.
Xiang, W., Lv, Q., Shi, H., Xie, B., Gao, L., 2020. Talanta 214, 120716.
Xu, B., Zheng, D., Qiu, W., Gao, F., Jiang, S., Wang, Q., 2015. Biosens. Bioelectron. 72, 175–181.
Xu, C., Cai, H., Xu, Q., He, P., Fang, Y., 2001. J. Anal. Chem. 369, 428–432.
Zargari, M., Sadeghi, M.R., Shahhosseiny, M.H., Kamali, K., Saliminejad, K., Esmaeilzadeh, A., Khorshid, H.R.K., 2011. Avicenna J. Med. Biotechnol. 3, 201.
Zhou, W., Wang, F., Ding, J., Liu, J., 2014. ACS Appl. Mater. Interfaces 6, 14795–14800.